Hyperspectral-Informed Sentinel-2-Based Monitoring of Paddy Residue Burning through Crop-State Discrimination

Rajkumar Dhakar
rajkumardhakar@iari.res.in
Indian Agricultural Research Institute
Vinay Kumar Sehgal
Indian Agricultural Research Institute
Sailja Rastogi
Indian Agricultural Research Institute
Niveta Jain
Indian Agricultural Research Institute
Rabi N. Sahoo
Indian Agricultural Research Institute

Research Article

Keywords: Biomass burning, Remote sensing, Agriculture, Fire, Crop residue

Posted Date: May 22nd, 2026

DOI: https://doi.org/10.21203/rs.3.rs-9513861/v1

Additional Declarations: No competing interests reported.

Hyperspectral-Informed Sentinel-2-Based Monitoring of Paddy Residue Burning through Crop-State Discrimination

Rajkumar Dhakar*, Vinay Kumar Sehgal*, Sailja Rastogi, Niveta Jain, Rabi N. Sahoo

Authors

(1) Rajkumar Dhakar*
Division of Agricultural Physics,
ICAR-Indian Agricultural Research Institute, New Delhi – 110012 INDIA
Email: rajkumardhakar@iari.res.in

(2) Vinay Kumar Sehgal*
Division of Agricultural Physics,
ICAR-Indian Agricultural Research Institute, New Delhi – 110012 INDIA
Email: sehgal@iari.res.in

(3) Sailja Rastogi
Division of Agricultural Physics,
ICAR-Indian Agricultural Research Institute, New Delhi – 110012 INDIA
Email: sailjarastogi4.gbpuat@gmail.com

(4) Niveta Jain
Division of Environment Science,
ICAR-Indian Agricultural Research Institute, New Delhi – 110012 INDIA
Email: nivetajain@gmail.com

(5) Ravi N. Sahoo
Division of Agricultural Physics,
ICAR-Indian Agricultural Research Institute, New Delhi – 110012 INDIA
Email: rnsahoo.iari@gmail.com

Graphical abstract

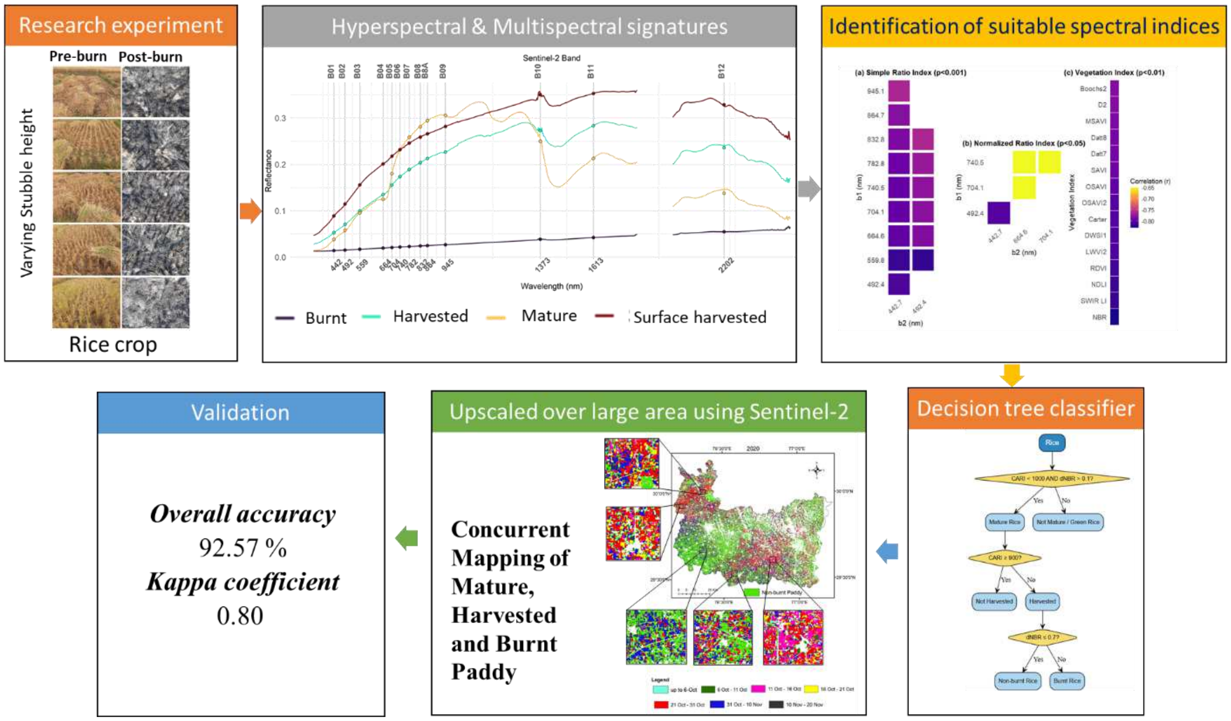

Abstract

Accurate mapping of agricultural residue burning using satellite data remains challenging due to the rapid temporal overlap and spectral similarity of mature crops, harvested fields, and burnt residues during peak harvest periods. This study presents a scalable, decision-rule–based methodology for the concurrent mapping of mature, harvested, and burnt paddy fields, integrating field-scale hyperspectral measurements with multi-temporal Sentinel-2 multispectral imagery. Hyperspectral observations captured systematic changes in crop reflectance associated with maturity, harvest intensity, and post-burn ash deposition, which were subsequently upscaled to Sentinel-2 spectral bands to evaluate a comprehensive set of vegetation and burn-sensitive indices. The analysis identified the Chlorophyll Absorption Ratio Index (CARI) as the most effective indicator for separating mature from harvested rice, while the delta Normalized Burn Ratio (dNBR) exhibited the highest sensitivity for distinguishing harvested fields from burnt residues. These indices were combined within a hierarchical decision-tree framework and applied to multi-date Sentinel-2 imagery to map rice burning dynamics across intensively cultivated districts in northern India. The approach achieved an overall classification accuracy of 92.57% with a kappa coefficient of 0.80, demonstrating strong spatial and temporal consistency with field observations.

By explicitly addressing intra-seasonal spectral confusion in agricultural landscapes, the proposed framework advances burned-area mapping beyond single-index detection toward integrated crop-state discrimination. The methodology is computationally efficient, sensor-transferable, and suitable for operational implementation, offering significant potential for large-scale agricultural monitoring, emission assessment, and policy-driven residue management in rice-based cropping systems globally.

Keywords: Biomass burning, Remote sensing, Agriculture, Fire, Crop residue

1. Introduction

India produces about 682.62 million tonnes (Mt) of dry crop residue annually from 11 major food crops, with 178.74 Mt deemed surplus and often unutilized (Jain et al., 2018). Managing this surplus is especially challenging in northwestern states under intensive rice-wheat systems. Due to short turnaround times, labor shortages, and lack of affordable alternatives, on-farm burning remains the most common disposal method (Jain et al., 2021). Despite its harmful environmental and health impacts, residue burning persists due to its ease and convenience, showing strong spatial and temporal variability. Effective government interventions depend on accurate, timely, and location-specific data—making satellite remote sensing a key tool for monitoring (Chawala & Sandhu, 2020; Kumar et al., 2019).

Traditional methods for estimating crop residue burning—based on expert judgment and generic emission coefficients—are often subjective and coarse (Andrae et al., 2001). Satellite remote sensing now enables consistent large-scale monitoring, with burned area mapping preferred over active fire events (AFEs), which may miss small or cloud-obscured fires or those outside satellite overpass times (McCarty et al., 2009). Burned area products like GLOBSCAR (Simon et al., 2004), L3JRC (Tansey et al., 2008) MCD45 (Roy et al., 2005), MCD64 (Chuvieco et al., 2018), and Fire_cci (Lizundia-Loiola et al., 2018), and MCD64A1 (Giglio et al., 2018) offer global coverage but at coarse resolutions (250 m–1 km), limiting their ability to detect small burn patches in croplands (Long et al., 2019). This highlights the need for high-resolution satellite data for accurate monitoring.

Satellite-based burnt area mapping uses two main types of spectral indices: burn-specific [e.g., Burnt Area Index (BAI) (Chuvieco et al., 2002; Sullivan et al., 2004), Normalized Burn Ratio

(NBR) (Key et al., 1999), and Mid-Infrared Burn Index (MIRBI) (Triggs and Flasse, 2001)] and general vegetation indices (e.g., NDVI) (Harris et al., 2011). Hybrid approaches, like region-specific thresholds on NBR (McCarty et al., 2009) and combined use of indices such as NDVI, NBR, and albedo (Kontoes et al., 2009), have improved accuracy. High-resolution multispectral imagery from both pre- and post-fire periods is crucial for detecting small, heterogeneous burn patches in croplands.

There is a need to improve the spatial resolution and classification accuracy of burnt area detection in agricultural landscapes. This is particularly challenging in croplands where mature, harvested, and burnt fields often coexist within narrow time windows and spatial proximity. Differentiating among these features using conventional burn indices or relying on single spectral indices often leads to confusion and misclassification. This study addresses this critical gap by systematically evaluating a suite of burn-sensitive and vegetation indices derived from hyperspectral reflectance characteristics and upscale it to large area using high-resolution multispectral satellite data (Sentinel-2 MSI). Our work focuses on developing a robust methodology to distinguish between mature paddy, harvested fields, and burnt residues three conditions that complicate remote detection. By integrating suite of spectral indices with pre- and post-burn imagery, we demonstrate a scalable framework for concurrent mapping of mature, harvested and burnt paddy using satellite data. The work offer potential to support policymakers and stakeholders with near-real-time, actionable insights for targeted interventions and residue management strategies. Additionally, this work supports broader goals in climate change mitigation, air quality improvement, and the advancement of sustainable agriculture in India and other similar agrarian regions globally.

2. Materials and Methods

2.1 Study Area

This study operated at two spatial scales: farm and regional. At the IARI research farm (coordinates: 28.080°N, 77.120°E), hyperspectral reflectance of paddy at different stages—green, mature, harvested, and burnt—was analyzed under experimental treatments (Figure 1a). Insights from this farm-level study informed a regional-scale assessment in Kaithal and Karnal (Haryana), testing the transferability of the algorithm to classify the paddy field conditions, especially burnt residues (Figure 1b). The region follows an intensive rice–wheat system, with sugarcane as a minor crop.

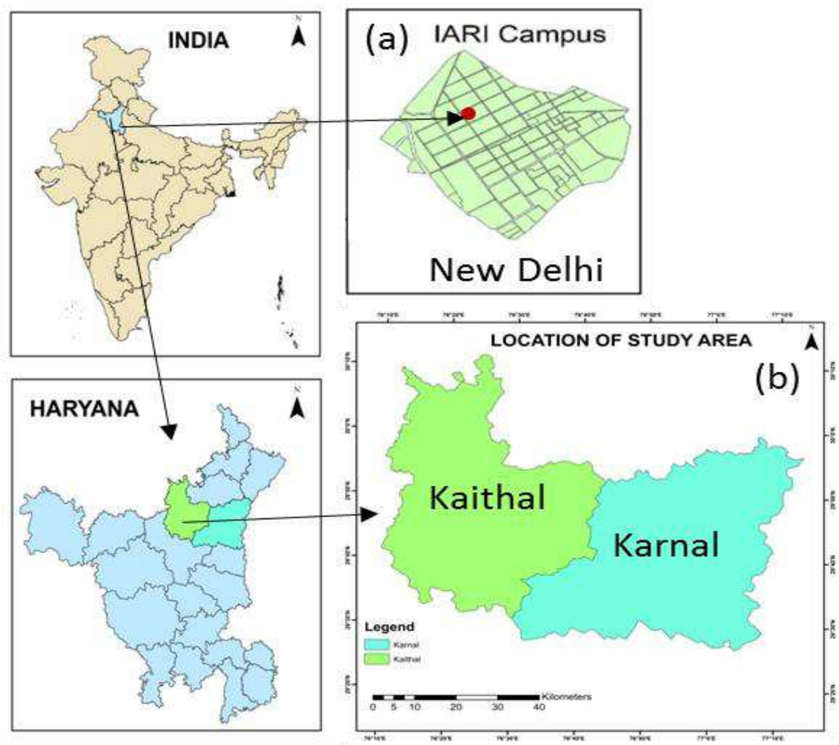

Figure 1: Study area (a) research farm, and (b) regional scale

2.2 Research farm scale

2.2.1 Experimental details

A field experiment was conducted with two rice varieties—Pusa Basmati-1409 and 1121—in $4 \times 5\ m^2$ plots with five replications. Standard crop practices were followed, and no major pest or disease issues occurred. To mimic typical stubble height variations post-harvest, crops were manually harvested on 17th November 2020 at six stubble heights: T1 (10 cm), T2 (20 cm), T3 (30 cm), T4 (40 cm), T5 (50 cm), and T6 (Control: surface harvested). Controlled burning was then performed on the remaining stubble for further analysis (Figure 2).

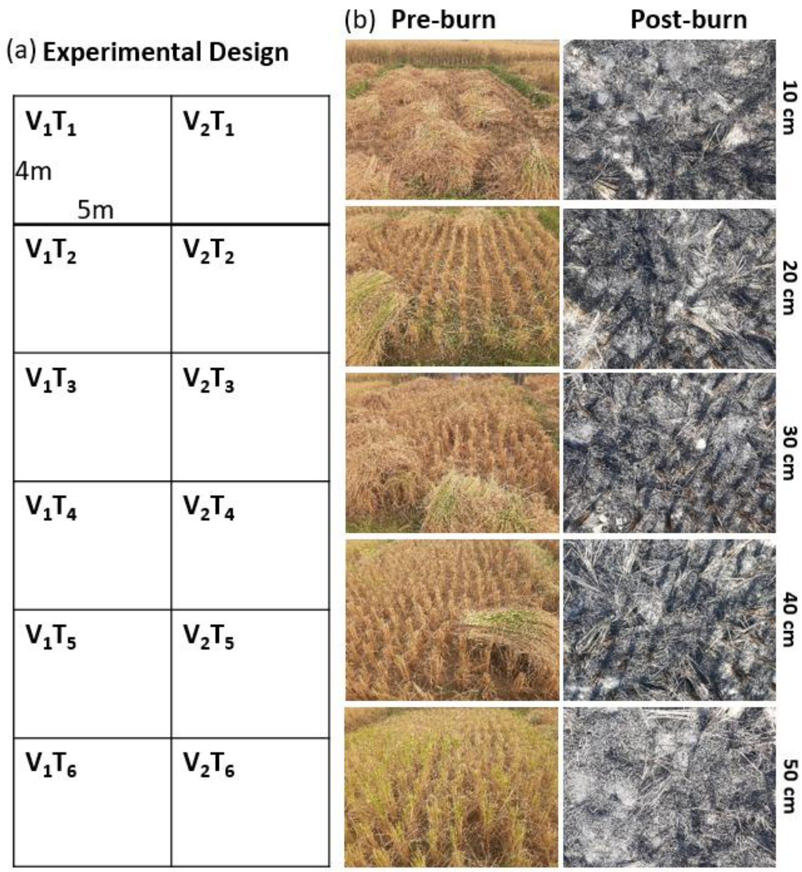

Figure 2: (a) Schematic layout of the experimental plots with different stubble height treatments. Dimensions are not to scale. V denotes rice variety (V1: Pusa Basmati-1409; V2: Pusa Basmati-1121), and T represents stubble height treatments (T1: 10 cm, T2: 20 cm, T3: 30 cm, T4: 40 cm, T5: 50 cm, T6: Control, i.e., surface harvested). (b) Representative photographs of each treatment during the pre-burn and post-burn phases.

2.2.2 Hyperspectral observations

To measure spectral reflectance in paddy fields, we used an ASD FieldSpec-3 spectroradiometer with a 25° field of view, measures reflectance across 350–2500 nm (VIS, NIR, SWIR) with 1.4 nm sampling. Data were interpolated to 1 nm intervals using ASD software. Measurements were conducted under clear sky conditions between 11:00 AM and 1:00 PM, with the sensor held perpendicular to the crop canopy and positioned to avoid shadow interference. Spectral reflectance data were collected on November 7, 24, and 29, 2020, corresponding to three distinct crop stages: mature crop, post-harvest stubble at varying heights, and post-burning residue. Each treatment was measured with three replications to ensure statistical reliability.

2.2.3 Processing of spectral observations

Spectroradiometric observations collected within each plot were averaged across wavelengths to generate representative spectral signatures for four distinct field feature classes: (1) mature paddy crop, (2) surface-harvested crop, (3) crop harvested at varying stubble heights, and (4) burnt crop residues. A suite of hyperspectral indices for each feature class were calculated using the 'hsdar' package in R statistical software, based on the hyperspectral reflectance data. Detailed descriptions of each hyperspectral index, along with their formulas and references, are summarized in Table S1.

We aggregated the 1 nm interval hyperspectral measurements into broadband reflectance values corresponding to the optical bands of the Sentinel-2A MSI sensor. This was accomplished using the sensor-specific Relative Spectral Response (RSR) functions, available from the Sentinel-2 user guide (https://sentinels.copernicus.eu/web/sentinel/user-guides/sentinel-2-msi/). The RSR functions provide wavelength-specific weighting factors for each MSI band across the 300–2600 nm range. The conversion was performed in R using the 'hsdar' package, enabling the generation of synthetic multispectral reflectance values for subsequent analysis and model development.

Pearson's correlation coefficients (r) were computed for three feature class combinations from 10 sample pairs: mature vs. harvested crops (r(Mature:Harvest)), mature vs. burnt crops (r(Mature:Burnt)), and harvested vs. burnt crops (r(Harvest:Burnt)) for both hyperspectral and multispectral data. Indices with statistically significant correlations ($p < 0.05$) were identified and analyzed to determine their potential for discriminating among these classes.

We calculated two types of multispectral indices—Simple Ratio (SR) and Normalized Ratio Index (NRI)—using all possible two-band combinations among the 13 spectral bands of Sentinel-2 MSI. This resulted in a total of 78 unique combinations. The indices were calculated using the following equations:

$$SR_{b1,b2} = \frac{R_{b1}}{R_{b2}}$$

$$NRI_{b1,b2} = \frac{R_{b1} - R_{b2}}{R_{b1} + R_{b2}}$$

Where, R_{b1} and R_{b2} represent reflectance values at Sentinel-2 MSI bands b1 and b2, respectively. The computation was performed using the 'hsdar' package in R.

In addition to SR and NRI, a set of burnt-specific multispectral indices—including Burn Area Index (BAI), Normalized Burn Ratio (NBR), and the Mid-Infrared Burn Index (MIRBI) and their change detection (dBAI, dNBR and dMIRBI) were also computed. The formulas and references for these indices are summarized in Table 2.

Table 2: Burnt-specific multispectral indices used in the study

Spectral Index	**Formula**	**Reference**
NBR	*(NIR-SWIR2)/(NIR+SWIR2)*	García and Caselles (1991)
BAI	$\frac{(1)}{\{(0.1+RED)^2+(0.06+NIR)^2\}}$	Chuvieco *et al.* (2002)
MIRBI	$10LSWIR - 9.8SSWIR + 2$	Triggs and Flasse (2001)

Following the burning of stubble in each plot, residue samples were collected, and the ash content (%) was quantified. Subsequently, Pearson's correlation coefficients were calculated between the ash content and all computed Simple Ratio (SR), Normalized Ratio Index (NRI) values derived from Sentinel-2 MSI bands and burnt-specific indices. Indices that exhibited statistically significant correlations ($p < 0.05$) were identified and considered useful for quantifying burn severity based on ash residue.

2.3 Regional level study

2.3.1 Ground truth data collection

A ground truth survey was conducted on November 6–7, 2020, coinciding with the rice harvest period, to identify three key field categories: mature rice, harvested fields, and burnt residue fields. Field coordinates were recorded using Garmin™ eTrex handheld GPS devices, and corresponding field boundaries were digitized on Google Earth in KML format.

2.3.2 Satellite data pre-processing

Thirteen cloud-free Sentinel-2 MSI images (10 m resolution) from September to November 2020 were obtained via the Copernicus Open Access Hub, covering rice maturity to harvest stages (Table S2). Image processing was done in ENVI/IDL™ 5.6, including mosaicking of two Sentinel-2 tiles (RFN and RFP), subsetting, and time-series stacking. A rice pixel mask was generated using supervised classification with ground truth samples, excluding non-rice areas from further analysis (Figure 3).

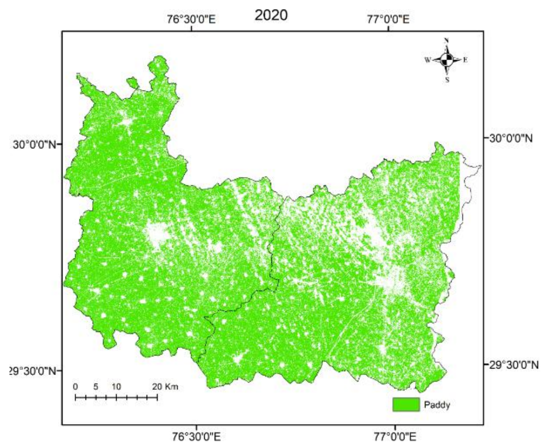

Figure 3: Classified rice map of regional level study area (Karnal and Kaithal districts of Haryana).

Based on hyperspectral insights, two spectral indices i.e. dNBR, and CARI were recognized as promising candidates to distinguish between mature and harvested fields and between harvested and burnt fields. To track progressive burning, dNBR was calculated using a pre-burning image (21 September 2020) and multiple post-burning images (1 October to 20 November 2020). A hierarchical rule-based classification, guided by a decision tree and using only rice pixels (from the rice mask), was applied in ENVI. The full methodology is outlined in Figure 4.

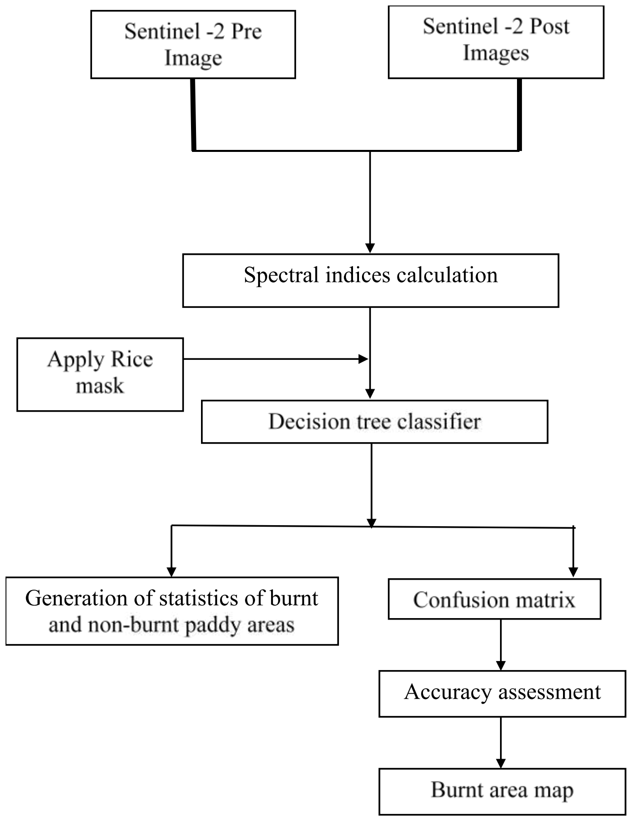

Figure 4: Flow chart of steps followed to map rice burnt area using pre and post burning images.

3. Results

3.1 Spectral characteristics of mature, harvested and burnt residue

The hyperspectral reflectance signatures of four feature classes—mature rice crop, pre-burnt rice crop (rice stubble harvested at varying heights), post-burnt rice crop (comprising black ash and unburnt residues), and surface-harvested rice crop (i.e., harvested at ground level, 0 cm)—revealed distinct spectral behavior across various regions of the electromagnetic spectrum (Figure 5). Mature and harvested crops exhibited clear separability in the red-edge, near-infrared (NIR), and shortwave infrared (SWIR) wavelength regions. However, spectral discrimination among these classes in the visible (VIS) range was limited due to overlapping reflectance characteristics.

Notably, post-burnt residues demonstrated a marked reduction in reflectance across the optical spectrum, enabling reliable differentiation from other surface classes. The spectral profile of surface-harvested treatments, dominated by exposed soil, exhibited characteristics typical of dry soil—namely, higher reflectance in the VIS and SWIR regions relative to mature and harvested crops, but lower reflectance in the NIR region compared to mature crop and higher than pre-burnt crop.

Among the spectral regions, the SWIR range between 1400–1800 nm showed the greatest inter-class variability, followed by the SWIR range between 2100–2400 nm. Correspondingly, multispectral reflectance profiles demonstrated similar trends to those observed in the hyperspectral signatures, further supporting the spectral separability of the feature classes (Figure 5).

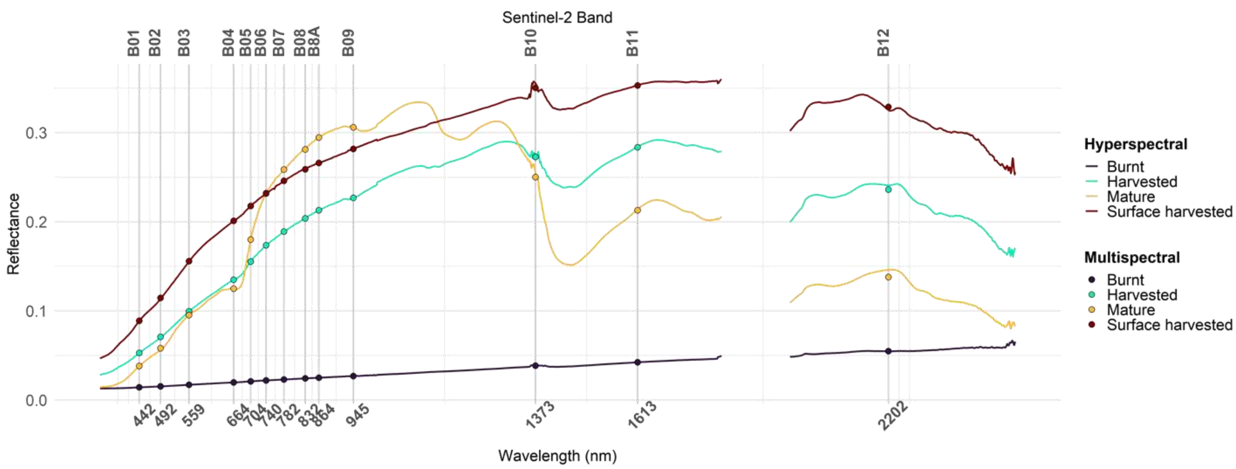

Figure 5: Hyperspectral and corresponding Sentinel-2 MSI multispectral signatures for pre-burnt (mature and harvested) and post burnt crops.

3.2 Effect of stubble height on hyperspectral signatures

The hyperspectral reflectance profiles of pre-burnt and post-burnt rice surfaces—harvested at stubble heights of 0, 10, 20, 30, 40, and 50 cm—are plotted in Figure 6. In the pre-burnt condition, reflectance decreased monotonically with increasing stubble height, but spectral curves for adjacent heights largely overlapped (Figure 6a). Only the 10 cm and 50 cm treatments were spectrally separable, with the 50 cm stubble exhibiting uniformly lower reflectance than the 10 cm stubble. Reflectance profiles for 10 cm and 20 cm stubble were essentially identical, as were those for 30 cm and 40 cm. Thus, smaller change in stubble height or crop residue does not lead to larger change in hyperspectral reflectance.

In contrast, the post-burnt treatments—regardless of stubble height—showed very low reflectance across the entire spectrum (VIS-SWIR) due to presence of dark ash (Figure 6b). There were subtle differences in reflectance in SWIR region due to stubble height, but no clear monotonic trend with stubble height. This suggests that the spectral behavior of burned residue is governed by a complex interplay of ash coverage, unburnt material, and potentially other surface properties.

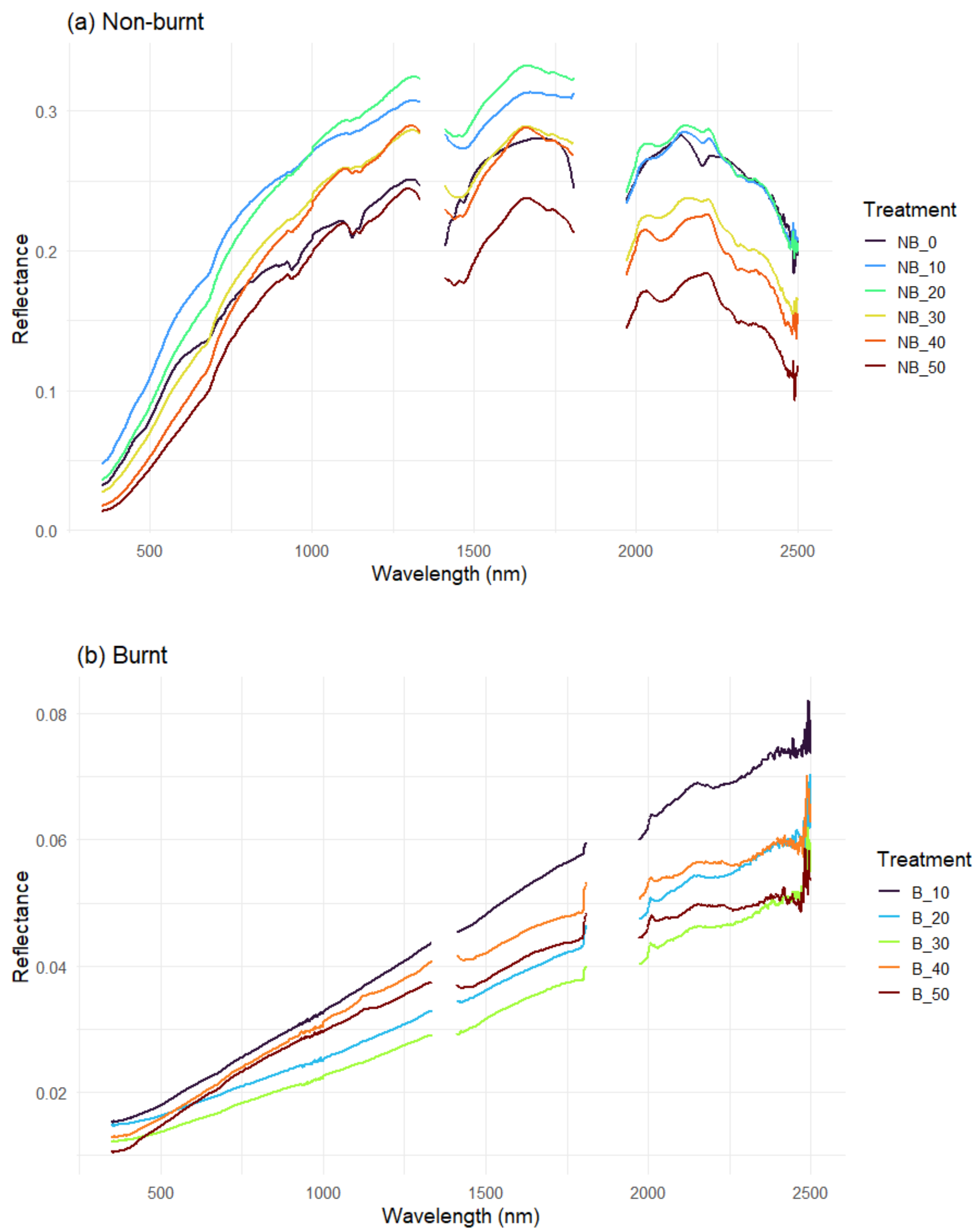

Figure 6: Hyperspectral reflectance profiles of (a) pre-burnt and (b) post-burnt rice surfaces at stubble heights of 0, 10, 20, 30, 40, and 50 cm (NB = non-burnt; B = burnt; NB_0 = surface-harvested).

3.3 Ash content in the burnt residues

Figure 7 presents the post-burning ash and unburnt residue proportions (%) for treatments with stubble heights of 10, 20, 30, 40, and 50 cm. Ash content ranged from 46 % to 70 %, whereas unburnt residue ranged from 30 % to 53 %. Although no strictly linear relationship was observed between stubble height and ash percentage, the 10 cm treatment produced the highest ash content (and lowest unburnt residue), while the 50 cm treatment exhibited the lowest ash content and highest unburnt residue. In general, increasing stubble height led to a greater proportion of unburnt material.

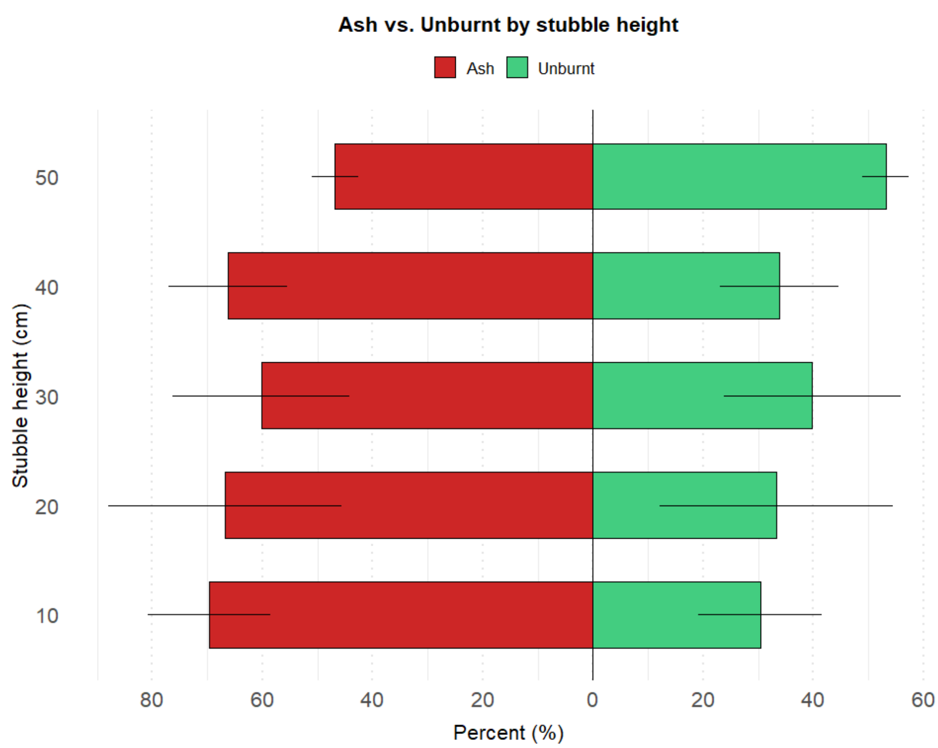

Figure 7: Post-burning proportions of ash content and unburnt residue across five stubble-height treatments (10, 20, 30, 40, and 50 cm).

3.3 Correlation between multispectral indices and ash content

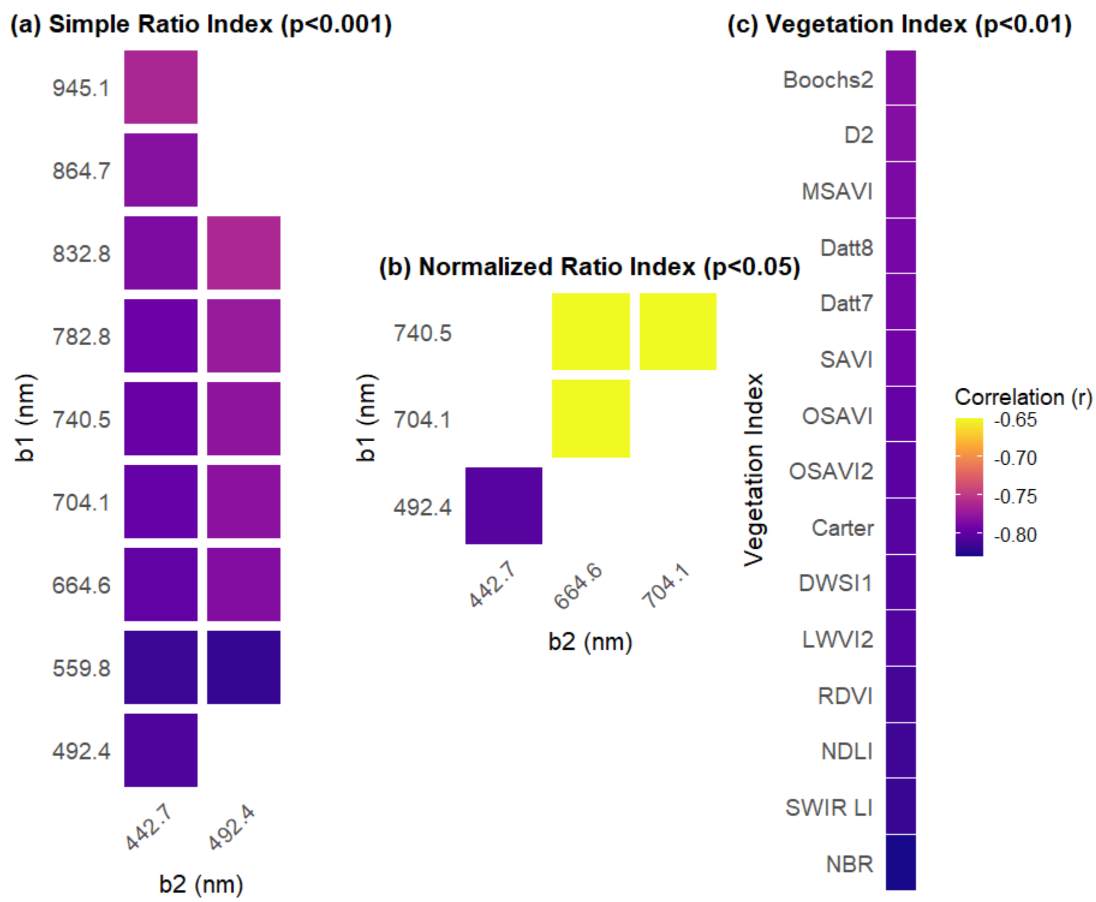

Figure 8: Pearson's correlation coefficients between post-burn ash content (%) and (a) Simple Ratio Indices (SRI) for various band combinations, (b) Normalized Ratio Indices (NRI) for various band combinations, and (c) selected vegetation indices. Only statistically significant correlations are displayed.

Three classes of multispectral indices—Simple Ratio Indices (SRI), Normalized Ratio Indices (NRI), and established vegetation indices—were evaluated for their correlation with post-burn ash content (%), with significant relationships plotted in Figure 8. Among SRIs, the ratio of green (559.8 nm) to blue (492.4 nm) reflectance exhibited the strongest negative correlation with ash percentage ($r = –0.82$, $p < 0.01$). Within the NRI group, the index derived from bands at 492.4 nm and 442.7 nm also showed a highly significant inverse association ($r = –0.80$, $p < 0.01$). Overall, ash content was predominantly negatively correlated with indices formulated from visible wavelengths.

Of the 121 hyperspectral indices tested, the Normalized Burn Ratio (NBR) achieved the highest significant negative correlation with ash content ($r = –0.83$, $p < 0.01$). It was closely followed by the Shortwave Infrared Linear Index (SWIR LI), the Normalized Difference Lignin Index (NDLI), and the Renormalized Difference Vegetation Index (RDVI).

3.4 Key Vegetation Indices for Distinguishing Mature, Harvested, and Burnt Crops

To differentiate mature from harvested crop, and harvested from burnt crop, Pearson correlations were calculated for published vegetation indices across these pairwise conditions [Mature: Harvest & Harvest: Burnt]. Five best spectral indices exhibiting statistically significant correlations ($p < 0.05$) for each pairwise condition is presented in Figure 9. The Chlorophyll Absorption Ratio Index (CARI) emerged as the most effective discriminator of mature versus harvested crop ($r = –0.74$), whereas the Normalized Burn Ratio (NBR) proved optimal for distinguishing harvested from burnt crop ($r = –0.83$).

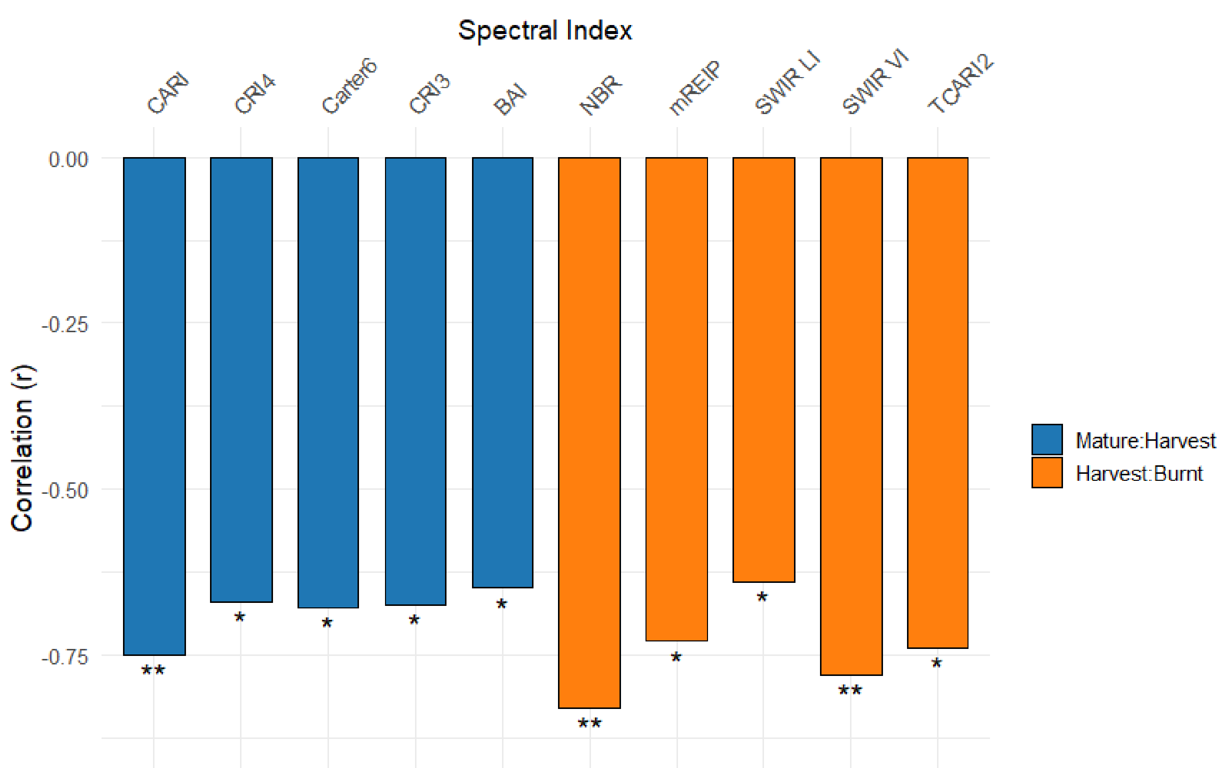

Figure 9: Pearson’s correlation coefficients between vegetation indices and crop conditions: (i) mature vs. harvested, and (ii) harvested vs. burnt. Asterisks denote significance levels (* $p < 0.05$; ** $p < 0.01$).

3.6 Change-detection spectral indices from mature to harvest and burnt

Three commonly cited change-detection indices—dNBR, dMIRBI, and dBAI—were computed to quantify spectral shifts from pre- to post-event (i.e., mature→harvest and mature→burnt), where "d" denotes the difference. Boxplots in Figure 10 display the interquartile ranges, minima, and maxima for both mature-to-harvest and mature-to-burnt transitions. Among the three, ΔNBR exhibited the greatest sensitivity to burning: its median value increased from 0.40 for mature→harvest to 0.75 for mature→burnt, with no overlap between the two distributions. In contrast, ΔMIRBI and ΔBAI showed wider variability and substantial overlap between their mature→harvest and mature→burnt values. Consequently, dNBR is the most reliable index for discriminating harvested from burnt crop using paired pre- and post-burn imagery.

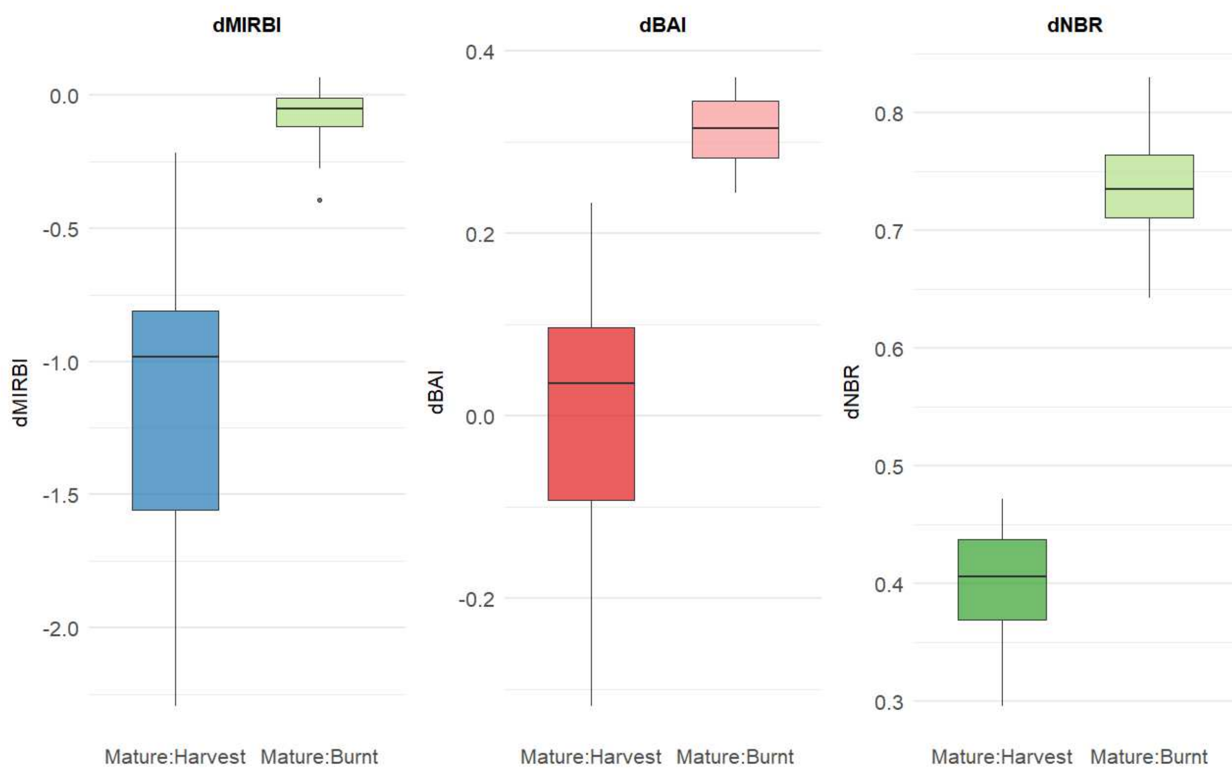

Figure 10: Comparison of changes in burn indices (dMIRBI, dBAI, and dNBR) from pre-burn (i.e. mature) to post-burnt (i.e. harvested or burnt)

3.7 Decision tree classifier for concurrent mapping of mature, harvested and burnt rice

Thresholds for CARI and dNBR were derived from ground-truth data to build a decision tree classifier in ENVI (Figure 11). The process began by masking non-rice areas, then excluded green rice using CARI ≥ 1000 and dNBR ≤ 0.10. Pixels with CARI ≥ 900 were labeled "Not Harvested." Remaining pixels were split into "Burnt" (dNBR > 0.7) and "Non-burnt" classes. This classifier was applied to Sentinel-2 images from 1 October to 20 November 2020 to track burning events in the study districts (Figure 12).

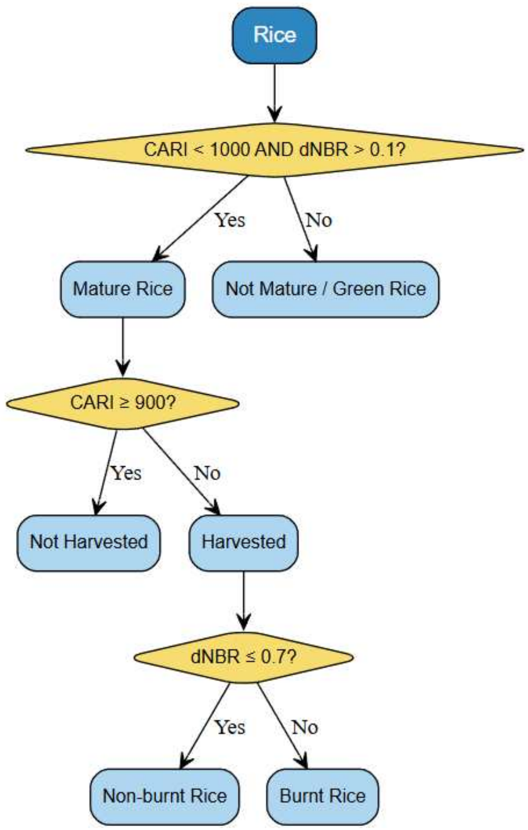

Figure 11: Decision tree classifier based on CARI and dNBR spectral indices to map burnt rice on different dates using Sentinel-2 MSI images.

The map highlights spatio-temporal variation in burnt areas, with peak burning between 21 October and 10 November 2020. Burning was more widespread in Karnal than in Kaithal. The final burnt rice map, validated with ground truth, showed 92.57% overall accuracy and a kappa coefficient of 0.80. Producer's accuracy exceeded 90% for both classes, while user's accuracy was 97.56% for non-burnt and 78.85% for burnt rice.

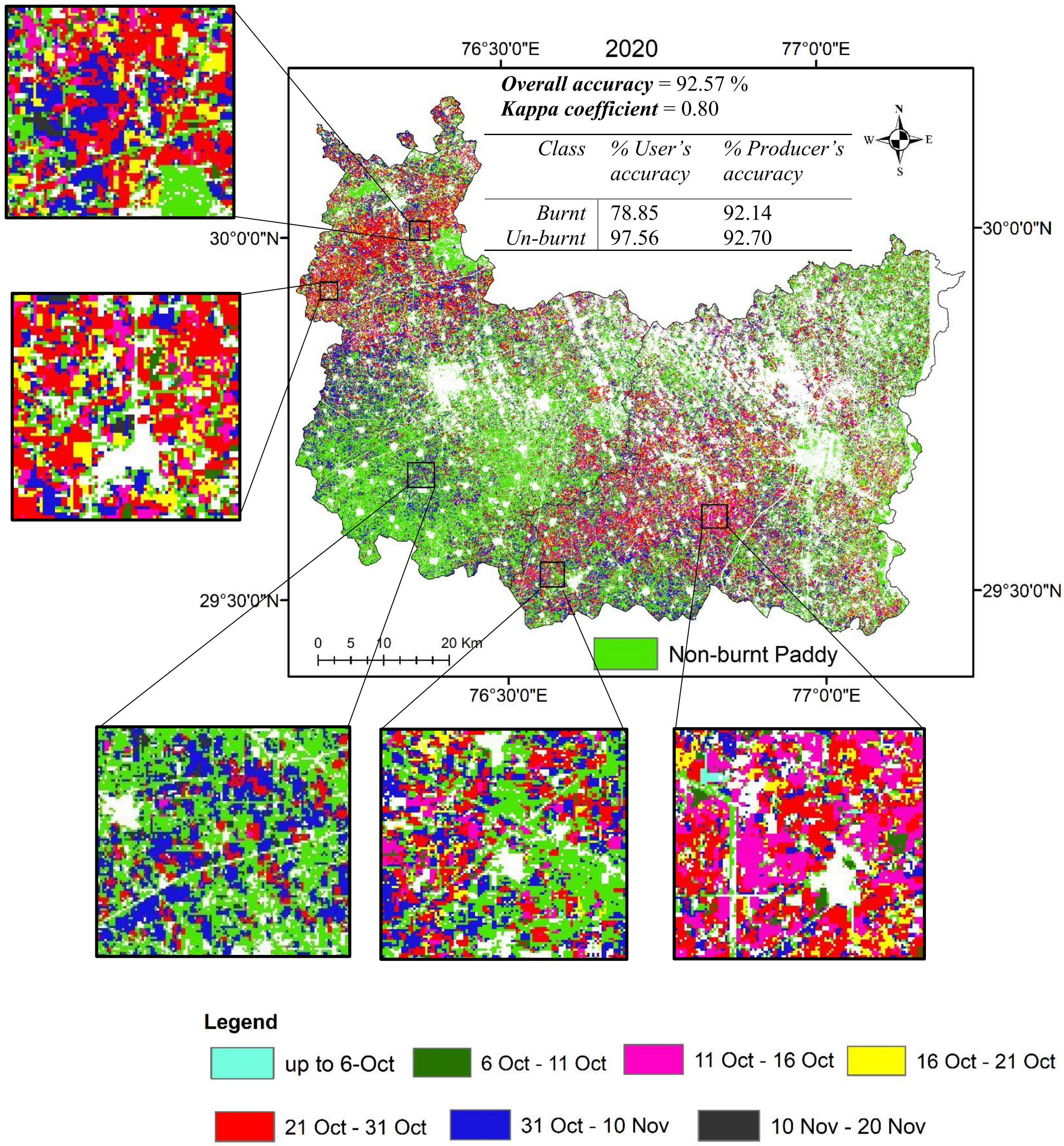

Figure 12: Map showing progress of rice burnt area in Kaithal and Karnal district of Haryana using multi-date Sentinel-2 MSI images. The inset shows details of map for sample areas.

4. Discussion

The reflectance decreases as paddy stubble height increases (350 nm to 2500 nm spectrum) due to factors like pigment absorption in the visible region, reduced internal reflection in the NIR region (due to less plant water content), and increased absorption in the SWIR region (due to more lignin and cellulose). This decrease may be associated with higher standing biomass and less exposure to soil background. Importantly, there are no previous studies demonstrating hyperspectral signatures of harvested paddy crops with varying stubble heights.

Burnt paddy residue, even with varying amounts of standing stubble, exhibited significantly reduced reflectance across all optical spectrum wavelengths compared to unburnt stubble. However, there were no distinctive hyperspectral signatures for different amounts of standing stubble in burnt residue. This suggests that even a small amount of ash leads to substantial energy absorption in the optical spectrum. The paddy burning resulted in darker colour carbonaceous ash than white ash. The lower visible region reflectance of the burnt surface is due to the darker ash deposition, which rarely exceeds 10 percent reflectance. This differs from previous studies in tropical savannah forests where recently burnt areas showed higher visible region reflectance compared to green forests and shrubs (Frederiksen et al., 1990; Langaas and Kane, 1991). The overall surface reflectivity increased if even moderately bright soil is exposed as a result of fire (Pereira et al., 1999). This contrast may be because, in our case, standing stubble had higher visible region reflectance than green vegetation, and the black soot or ash from burning covered the underlying soil more extensively, reducing overall reflectance.

Mapping burnt fields via satellite remote sensing is challenging due to the simultaneous presence of mature crop, harvested crop, and burnt fields, which are hard to differentiate using single spectral indices. This study aimed to develop algorithm for concurrent mapping of green, mature, harvested and burnt rice by exploring various multi-spectral indices derived from hyperspectral data, particularly Sentinel-2 MSI bands. The results revealed that the Chlorophyll Absorption Ratio Index (CARI) was the most effective index for distinguishing between mature and harvested crops. CARI, calculated using green, red, and red edge wavelengths (550 nm, 670 nm, and 700 nm), demonstrated a notable capacity to differentiate between these categories of rice. Mature crops had lower reflectance in green and red bands but higher reflectance in the red edge band compared to harvested crops, resulting in significantly lower CARI values for mature crops. Although CARI is traditionally a greenness index used for estimating photosynthetic activity (Kim et al. 1994), but this study found it to be remarkably suitable for discriminating between mature and harvested rice crops, with no previous reports of CARI's potential for this purpose.

Paddy residue burning results in black coloration of the field, which can be detected and assessed by remote sensing data (Singh et al., 2009). We found that well known burn index i.e. NBR (normalized burn ratio) showed highly significant negative correlation with % ash ($r = -0.83$) at $p < 0.01$ followed by SWIR LI, NDLI and RDVI. Robichaud et al. (2007) also reported significant negative correlation between percent ash and NBR. The high correlation of NBR with ash also indicated that the portion of residue was burnt with high burnt severity. It was observed that NBR was found to be most suitable to distinguish between harvest and burnt crop based on the correlation of NBR of harvested crop and NBR of burnt crop.

In general, burnt area mapping is being done based on change detection methods which include pre-burn and post-burn images (Miller and Thode, 2007). The change detection method exploits the fact that residue burning drastically changes the spectral characteristics of the surface and by inspecting at pre-burn and post-burn conditions, these changes can be ascertained with confidence. Therefore, we evaluated the change in burn indices like dNBR, dMIRBI and dBAI based on training signature. Among the three burnt indices, dNBR found to be more sensitive to change between pre-burn to post-burn situation. The reason of NBR demonstrating good performance maybe due to the use of NIR band which is sensitive to burnt area as NIR reflectance reduces significantly after burning. Our results agree with the findings of Schepers et al. (2014) and Harris et al. (2011) which showed that NBR using the band combination of SWIR and NIR wavebands are considered to be sensitive to post fire reflectance changes. However, the study done by Lu et al. (2016) shows that MIRBI which is derived by the band combination of two SWIR bands have better separability for immediate post-burnt area estimation, often superior to extensively used NBR. Some studies concluded that spectral indices relying on visible region and near infrared region are the better discriminators of burnt area, if employed immediately after burning event takes place, whereas those spectral indices which use the shortwave infrared region of electromagnetic spectrum that lies in between 1100 and 3000 nm to be more suitable to map long term effects of fire on vegetation (Lozano et al., 2012; Pickell et al., 2016 and Hislop et al., 2018). Our results do not corroborate with the key findings of Mpakairi et al. (2020) who calculated eight spectral indices using Sentinel-2 MSI imagery and their results showed that BAI and GEMI outperformed other indices with an accuracy greater than 0.90. The accuracy of NBR was found to be 0.76 which is lowest among all the spectral indices used. These results follow the recommendations of Adelabu et al. (2014) showing that red-edge is sensitive to chlorophyll changes. These chlorophyll alterations are typical in burned areas (Ngadze et al., 2020) and hence using the red edge spectral band instead of traditional red band could help locate burnt areas with better accuracy. These arguments show that our results support as well as contradict previous studies reported in literature. These differences may be the results of the changes in various factors that include vegetation types, climatic conditions and elevation as well as time of burnt area mapping. Most of these studies analyzed the burning of forest areas while our study was confined to crop residue burning.

Discrimination of burnt and non-burnt based on dNBR is usually done by fixing a threshold value. The identification of threshold value is critical for classification accuracy. We fixed the threshold value of dNBR based on values calculated from ground truth sites. Mapping of burnt area merely based on thresholds of dNBR may lead to relatively inaccurate result, therefore we devised a hierarchical decision tree algorithm for mapping of burnt area. We obtained 92.57% classification accuracy in the paddy burnt area mapping, it shows the robustness of the devised algorithm and has potential to be adopted in operational schemes needed information on spatiotemporal patterns of crop residue burning.

5. Conclusions

This study demonstrates that reliable detection of crop residue burning in intensively managed agricultural systems requires explicit discrimination between mature crops, harvested fields, and burnt residues rather than reliance on standalone burn indices. Field-based hyperspectral measurements revealed consistent spectral contrasts among these crop states, particularly across the red-edge, near-infrared, and shortwave-infrared regions, enabling their systematic translation to multispectral satellite observations.

Among the indices evaluated, CARI emerged as a robust indicator of crop physiological status, enabling stable separation of mature and harvested rice, while dNBR provided strong sensitivity to residue burning severity and ash presence. The integration of these indices within a hierarchical decision-tree classifier allowed simultaneous mapping of crop condition and burning dynamics using multi-temporal Sentinel-2 imagery, achieving high classification accuracy at the regional scale.

Importantly, the resulting maps provide more than retrospective burned-area estimates; they enable identification of spatial patterns of harvest progression and zones with elevated likelihood of burning. This capability enhances the utility of satellite remote sensing for anticipatory monitoring, supporting targeted mitigation strategies, improved emission inventories, and informed deployment of residue-management interventions. Given its reliance on freely available data and physically interpretable decision rules, the proposed framework is well suited for operational adoption and extension to other rice-dominated agroecosystems facing similar residue-burning challenges.

Acknowledgements

Authors acknowledge the research facilities extended by Head, Division of Agricultural Physics, Indian Agricultural Research Institute, New Delhi.

Funding Support

This work is supported through the research project under Crop Residue Management component of PM-Rastriya Krishi Vikas Yojana (RKVY) scheme of Ministry of Agriculture & Farmers' Welfare, Government of India, along with partial funding from an IARI in-house project [Project code: CRSCIARISIL20210034319].

CRediT authorship contribution statement

Rajkumar Dhakar: Writing – review & editing, Writing – original draft, Validation, Methodology, Investigation, Formal analysis, Data curation. **Vinay Kumar Sehgal:** Writing – review & editing, Supervision, Methodology, Funding acquisition, Formal analysis, Conceptualization. **Sailja Rastogi:** Methodology, Investigation, Formal analysis, Data curation. **Niveta Jain:** Writing – review & editing. **Rabi N Sahoo:** Writing – review & editing, Investigation, Data curation.

References

Adelabu, S., Mutanga, O., & Adam, E. (2014). Evaluating the impact of red-edge band from Rapideye image for classifying insect defoliation levels. *ISPRS Journal of Photogrammetry and Remote Sensing*, *95*, 34-41.

Andreae, M. O., & Merlet, P. (2001). Emission of trace gases and aerosols from biomass burning. *Global biogeochemical cycles*, *15*(4), 955-966.
Andreae, M. O., & Merlet, P. (2001). Emission of trace gases and aerosols from biomass burning. *Global biogeochemical cycles*, *15*(4), 955-966.
Apan, A., Held, A., Phinn, S., & Markley, J. (2004). Detecting sugarcane 'orange rust'disease using EO-1 Hyperion hyperspectral imagery. *International Journal of Remote Sensing*, *25*(2), 489-498

Boochs, F., Kupfer, G., Dockter, K., & Kühbauch, W. (1990). Shape of the red edge as vitality indicator for plants. *Remote Sensing*, *11*(10), 1741-1753.

Carter, G. A. (1994). Ratios of leaf reflectances in narrow wavebands as indicators of plant stress. *Remote sensing*, *15*(3), 697-703.

Chawala, P., & Sandhu, H. A. S. (2020). Stubble burn area estimation and its impact on ambient air quality of Patiala & Ludhiana district, Punjab, India. *Heliyon*, *6*(1), e03095.

Cho, M. A., & Skidmore, A. K. (2006). A new technique for extracting the red edge position from hyperspectral data: The linear extrapolation method. *Remote Sensing of Environment*, *101*(2), 181-193.

Chuvieco, E., Aguado, I., Yebra, M., Nieto, H., Salas, J., Martín, M. P., ... & Zamora, R. (2010). Development of a framework for fire risk assessment using remote sensing and geographic information system technologies. *Ecological Modelling*, *221*(1), 46-58.

Chuvieco, E., Lizundia-Loiola, J., Pettinari, M. L., Ramo, R., Padilla, M., Tansey, K., ... & Plummer, S. (2018). Generation and analysis of a new global burned area product based on MODIS 250 m reflectance bands and thermal anomalies. *Earth System Science Data*, *10*(4), 2015-2031.

Chuvieco, E., Martin, M. P., & Palacios, A. (2002). Assessment of different spectral indices in the red-near-infrared spectral domain for burned land discrimination. *International Journal of Remote Sensing*, *23*(23), 5103-5110.
Chuvieco, E., Martin, M. P., & Palacios, A. (2002). Assessment of different spectral indices in the red-near-infrared spectral domain for burned land discrimination. *International Journal of Remote Sensing*, *23*(23), 5103-5110.
Crutzen, P. J., & Andreae, M. O. (1990). Biomass burning in the tropics: Impact on atmospheric chemistry and biogeochemical cycles. *Science*, *250*(4988), 1669-1678.

Datt, B. (1999). Remote sensing of water content in Eucalyptus leaves. *Australian Journal of Botany*, *47*(6), 909-923.

Elvidge, C. D., & Chen, Z. (1995). Comparison of broad-band and narrow-band red and near-infrared vegetation indices. *Remote Sensing of Environment*, *54*(1), 38-48.

Filella, I., & Penuelas, J. (1994). The red edge position and shape as indicators of plant chlorophyll content, biomass and hydric status. *International Journal of Remote Sensing*, *15*(7), 1459-1470.

Frederiksen, P., Langaas, S., & Mbaye, M. (1990). NOAA-AVHRR and GIS-based monitoring of fire activity in Senegal—a provisional methodology and potential applications. In: Goldammer J.G. (eds.), *Fire in the Tropical Biota,* Vol 84, Springer, Berlin, Heidelberg, 400-417.

Galvao, L. S., Formaggio, A. R., & Tisot, D. A. (2005). Discrimination of sugarcane varieties in Southeastern Brazil with EO-1 Hyperion data. *Remote Sensing of Environment*, *94*(4), 523-534.

García, M. L., & Caselles, V. (1991). Mapping burns and natural reforestation using Thematic Mapper data. *Geocarto International*, *6*(1), 31-37.
García, M. L., & Caselles, V. (1991). Mapping burns and natural reforestation using Thematic Mapper data. *Geocarto International*, *6*(1), 31-37.
Giglio, L., Boschetti, L., Roy, D. P., Humber, M. L., & Justice, C. O. (2018). The Collection 6 MODIS burned area mapping algorithm and product. *Remote Sensing of Environment*, *217*, 72-85.

Gitelson, A. A., Buschmann, C., & Lichtenthaler, H. K. (1999). The chlorophyll fluorescence ratio F735/F700 as an accurate measure of the chlorophyll content in plants. *Remote Sensing of Environment*, *69*(3), 296-302.

Harris, S., Veraverbeke, S., & Hook, S. (2011). Evaluating spectral indices for assessing fire severity in chaparral ecosystems (Southern California) using MODIS/ASTER (MASTER) airborne simulator data. *Remote sensing*, *3*(11), 2403-2419.
Harris, S., Veraverbeke, S., & Hook, S. (2011). Evaluating spectral indices for assessing fire severity in chaparral ecosystems (Southern California) using MODIS/ASTER (MASTER) airborne simulator data. *Remote sensing*, *3*(11), 2403-2419.

Hislop, S., Jones, S., Soto-Berelov, M., Skidmore, A., Haywood, A., & Nguyen, T. H. (2018). Using Landsat spectral indices in time-series to assess wildfire disturbance and recovery. *Remote Sensing*, *10*(3), 460.

Huete, A. R. (1988). A soil-adjusted vegetation index (SAVI). *Remote Sensing of Environment*, *25*(3), 295-309.

Jain, N., Sehgal, V.K., Pathak, H., Kumar, O., Dhakar, R. (2021). Greenhouse gas and particulate matter emissions from rice residue burning in Punjab and Haryana states of India. *In book: Biomass Burning in South and Southeast Asia: Impacts on Biosphere,* Vol 2, CRC Press, 171-190.

Jain, N., Sehgal, V.K., Singh, S., Kaushik, N. (2018). Estimation of surplus crop residue in India for biofuel production. *Joint Report of TIFAC and IARI*, published by Technology Information, Forecasting & Assessment Council, New Delhi, India, p 437.

Kasischke, E. S., Hewson, J. H., Stocks, B., van der Werf, G., & Randerson, J. (2003). The use of ATSR active fire counts for estimating relative patterns of biomass burning–a study from the boreal forest region. *Geophysical Research Letters*, *30*(18).

Key, C.H.; Benson, N.C. (1999). The Normalized Burn Ratio (NBR): A Landsat TM Radiometric Measure of Burn Severity. *United States Geological Survey*, Northern Rocky Mountain Science Center: Bozeman, MT, USA.

Kim, M. S., Daughtry, C. S. T., Chappelle, E. W., McMurtrey, J. E., & Walthall, C. L. (1994, January). The use of high spectral resolution bands for estimating absorbed photosynthetically active radiation (A par). In *CNES, Proceedings of 6th International Symposium on Physical Measurements and Signatures in Remote Sensing*.

Kontoes, C. C., Poilvé, H., Florsch, G., Keramitsoglou, I., & Paralikidis, S. (2009). A comparative analysis of a fixed thresholding vs. a classification tree approach for operational burn scar detection and mapping. *International Journal of Applied Earth Observation and Geoinformation*, *11*(5), 299-316.

Kumar, P., Rajpoot, S. K., Jain, V., Saxena, S., & Ray, S. S. (2019). Monitoring of rice crop in Punjab and Haryana with respect to residue burning. *International Archives of the Photogrammetry, Remote Sensing & Spatial Information Sciences*, Volume XLII-3/W6.

Langaas, S. & Kane, R. (1991). Temporal spectral signatures of fire scars in savanna woodland. In *IGARSS'91 Proceedings - Remote Sensing: Global Monitoring for Earth Management,* Vol. 3, pp. 1157-1160.

Lizundia-Loiola, J., Pettinari, M. L., Chuvieco, E., Storm, T., & Gómez-Dans, J. (2018). ESA CCI ECV Fire Disturbance: Algorithm Theoretical Basis Document-MODIS, version 2.0.

Lobell, D. B., Asner, G. P., Law, B. E., & Treuhaft, R. N. (2001). Subpixel canopy cover estimation of coniferous forests in Oregon using SWIR imaging spectrometry. *Journal of Geophysical Research: Atmospheres*, *106*(D6), 5151-5160.

Lozano, F. Javier, Susana Suárez-Seoane, and Estanislao de Luis-Calabuig. (2012). Does fire regime affect both temporal patterns and drivers of vegetation recovery in a resilient Mediterranean landscape? A remote sensing approach at two observation levels. *International Journal of Wildland Fire*, *21*(6): 666-679.

Martín, M. P., Gómez, I., & Chuvieco, E. (2006). Burnt Area Index (BAIM) for burned area discrimination at regional scale using MODIS data. *Forest Ecology and Management*, (234), S221.

McCarty, J. L., Korontzi, S., Justice, C. O., & Loboda, T. (2009). The spatial and temporal distribution of crop residue burning in the contiguous United States. *Science of the Total Environment*, *407*(21), 5701-5712.

Miller, J. D., & Thode, A. E. (2007). Quantifying burn severity in a heterogeneous landscape with a relative version of the delta Normalized Burn Ratio (dNBR). *Remote Sensing of Environment*, *109*(1), 66-80.

Mpakairi, K. S., Ndaimani, H., & Kavhu, B. (2020). Exploring the utility of Sentinel-2 MSI derived spectral indices in mapping burned areas in different land-cover types. *Scientific African*, *10*, e00565.

Ngadze, F., Mpakairi, K. S., Kavhu, B., Ndaimani, H., & Maremba, M. S. (2020). Exploring the utility of Sentinel-2 MSI and Landsat 8 OLI in burned area mapping for a heterogenous savannah landscape. *Plos One*, *15*(5), e0232962.

Pereira, J.M.C., Sa, A.C.L., Sousa, A.M.O., Martín, M.P., Chuvieco, E. 1999. Regional-scale burnt area mapping in Southern Europe using NOAA-AVHRR 1 km data. In Chuvieco,

E. (Ed.) *Remote Sensing of Large Wildfires in the European Mediterranean Basin*. Berlin, Springer-Verlag:139-155.

Pickell, P. D., Hermosilla, T., Frazier, R. J., Coops, N. C., & Wulder, M. A. (2016). Forest recovery trends derived from Landsat time series for North American boreal forests. *International Journal of Remote Sensing*, *37*(1), 138-149.

Qi, J., Chehbouni, A., Huete, A. R., Kerr, Y. H., & Sorooshian, S. (1994). A modified soil adjusted vegetation index. *Remote sensing of Environment*, *48*(2), 119-126.

Robichaud, P. R., Lewis, S. A., Laes, D. Y., Hudak, A. T., Kokaly, R. F., & Zamudio, J. A. (2007). Postfire soil burn severity mapping with hyperspectral image unmixing. *Remote Sensing of Environment*, *108*(4), 467-480.

Rondeaux, G., Steven, M., & Baret, F. (1996). Optimization of soil-adjusted vegetation indices. *Remote Sensing of Environment*, *55*(2), 95-107.

Roujean, J. L., & Breon, F. M. (1995). Estimating PAR absorbed by vegetation from bidirectional reflectance measurements. *Remote Sensing of Environment*, *51*(3), 375-384.

Roy, D. P., Jin, Y., Lewis, P. E., & Justice, C. O. (2005). Prototyping a global algorithm for systematic fire-affected area mapping using MODIS time series data. *Remote Sensing of Environment*, *97*(2), 137-162.

Schepers, L., Haest, B., Veraverbeke, S., Spanhove, T., Vanden Borre, J., & Goossens, R. (2014). Burned area detection and burn severity assessment of a heathland fire in Belgium using airborne imaging spectroscopy (APEX). *Remote Sensing*, *6*(3), 1803-1826.

Scholes, R. J., Kendall, J., & Justice, C. O. (1996). The quantity of biomass burned in southern Africa. *Journal of Geophysical Research: Atmospheres*, *101*(D19), 23667-23676.

Serrano, L., Penuelas, J., & Ustin, S. L. (2002). Remote sensing of nitrogen and lignin in Mediterranean vegetation from AVIRIS data: Decomposing biochemical from structural signals. *Remote Sensing of Environment*, *81*(2-3), 355-364.

Simon, M., Plummer, S., Fierens, F., Hoelzemann, J. J., & Arino, O. (2004). Burnt area detection at global scale using ATSR-2: The GLOBSCAR products and their qualification. *Journal of Geophysical Research: Atmospheres*, *109*(D14).

Singh, G., Kant, Y., & Dadhwal, V. K. (2009). Remote sensing of crop residue burning in Punjab (India): a study on burned area estimation using multi-sensor approach. *Geocarto International*, *24*(4), 273-292.

Sullivan, D. G., Shaw, J. N., Mask, P. L., Rickman, D., Guertal, E. A., Luvall, J., & Wersinger, J. M. (2004). Evaluation of multispectral data for rapid assessment of wheat straw residue cover. *Soil Science Society of America Journal*, *68*(6), 2007-2013.

Tansey, K., Grégoire, J. M., Defourny, P., Leigh, R., Pekel, J. F., Van Bogaert, E., & Bartholomé, E. (2008). A new, global, multi-annual (2000–2007) burnt area product at 1 km resolution. Geophysical Research Letters, 35(L01401), 1-6.

Trigg, S., & Flasse, S. (2001). An evaluation of different bi-spectral spaces for discriminating burned shrub-savannah. *International Journal of Remote Sensing*, *22*(13), 2641-2647.

Vadrevu, K. P., Lasko, K., Giglio, L., & Justice, C. (2014). Analysis of Southeast Asian pollution episode during June 2013 using satellite remote sensing datasets. *Environmental Pollution*, *195*, 245-256.

Van der Werf, G. R., Randerson, J. T., Giglio, L., Collatz, G. J., Mu, M., Kasibhatla, P. S., ... & van Leeuwen, T. T. (2010). Global fire emissions and the contribution of deforestation, savanna, forest, agricultural, and peat fires (1997–2009). Atmospheric chemistry and physics, 10(23), 11707-11735.

Wu, C., Niu, Z., Tang, Q., & Huang, W. (2008). Estimating chlorophyll content from hyperspectral vegetation indices: Modeling and validation. *Agricultural and Forest Meteorology*, *148*(8-9), 1230-1241.

Zarco-Tejada, P. J., Pushnik, J. C., Dobrowski, S., & Ustin, S. L. (2003). Steady-state chlorophyll a fluorescence detection from canopy derivative reflectance and double-peak red-edge effects. *Remote Sensing of Environment*, *84*(2), 283-294.

Supplementary Files

This is a list of supplementary files associated with this preprint. Click to download.

- Supplementarymaterial.docx